LICENTIATE THESIS

Synthesis and Characterisation of High Entropy Alloy and Coating

Sajid Ali Alvi

Engineering Materials

LULEÅ UNIVERSITY OF TECHNOLOGY

Licentiate thesis

Synthesis and Characterisation of High Entropy Alloy and Coating

Sajid Ali Alvi

Department of Engineering Sciences and Mathematics

Division of Materials Science

Luleå University of Technolgy

Printed by Luleå University of Technology, Graphic Production 2019

ISSN 1402-1757
ISBN 978-91-7790-394-9 (print)
ISBN 978-91-7790-395-6 (pdf)

Luleå 2019

www.ltu.se

Abstract

High entropy alloys (HEAs) are a new class of alloys that contains five or more principal elements in equiatomic or near-equiatomic proportional ratio. The configuration entropy in the HEAs tends to stabilize the solid solution formation, such as body-centered-cubic (BCC), face-centered-cubic (FCC) and/or hexagonal-closed-pack (HCP) solid solution. The high number of principal elements present in HEAs results in severe lattice distortion, which in return gives superior mechanical properties compared to the conventional alloys. HEAs are considered as a paradigm shift for the next generation high temperature alloys in extreme environments, such as aerospace, cutting tools, and bearings applications.

The project is based on the development of refractory high entropy alloy and film. The first part of the project involves designing high entropy alloy of CuMoTaWV using spark plasma sintering (SPS) at 1400 ^{o}C. The sintered alloy showed the formation of a composite of BCC solid solution (HEA) and V rich zones with a microhardness of 600 HV and 900 HV, respectively. High temperature ball-on-disc tribological studies were carried out from room temperature (RT) to 600 ^{o}C against Si_3N_4 counter ball. Sliding wear characterization of the high entropy alloy composite showed increasing coefficient of friction (COF) of 0.45-0.67 from RT to 400 ^{o}C and then it decreased to 0.54 at 600 ^{o}C. The wear rates were found to be low at RT (4×10^{-3} mm^3/Nm) and 400 ^{o}C (5×10^{-3} mm^3/Nm) and slightly high at 200 ^{o}C (2.3×10^{-2} mm^3/Nm) and 600 ^{o}C (4.5×10^{-2} mm^3/Nm). The tribology tests showed adaptive behavior with lower wear rate and COF at 400 ^{o}C and 600 ^{o}C, respectively. The adaptive wear behavior at 400 ^{o}C was due to the formation of CuO that protected against wear, and at 600 ^{o}C, the V-rich zones converted to elongated magneli phases of V_2O_5 and helped in reducing the friction coefficient.

The second part of the project consists of sintering of novel CuMoTaWV target material using SPS and depositing CuMoTaWV refractory high entropy films (RHEF) using DC-

magnetron sputtering on silicon and 304 stainless steel substrate. The deposited films showed the formation of nanocrystalline BCC solid solution. The X-ray diffraction (XRD) studies showed a strong (110) preferred orientation with a lattice constant and grain size of 3.18 Å and 18 nm, respectively. The lattice parameter were found to be in good agreement with the one from the DFT optimized SQS (3.16 Å). The nanoindentation hardness measurement at 3 mN load revealed an average hardness of 19 ± 2.3 GPa and an average Young's modulus of 259.3 ± 19.2 GPa. The Rutherford backscattered (RBS) measurement showed a gradient composition in the cross-section of the film with W, Ta and Mo rich at the surface, while V and Cu were found to be rich at the substrate-film interface. AFM measurements showed an average surface roughness (Sa) of 3 nm. Nano-pillars of 440 nm diameter from CuMoTaWV RHEFs were prepared by ion-milling in a focused-ion-beam (FIB) instrument, followed by its compression. The compressional yield strength and Young's modulus was calculated to be 10.7 ± 0.8 GPa and 196 ± 10 GPa, respectively. Room temperature ball-on-disc tribological test on the CuMoTaWV RHEF, after annealing at 300 ^{o}C, against E52100 alloy steel (Grade 25, 700-880 HV) showed a steady state COF of 0.25 and a low average wear rate of 6.4 x 10^{-6} mm^3/Nm.

Acknowledgements

This licentiate thesis is part of the project “thermo-mechanical and tribology infrastructure (TMTEST)” which is focused on the development of new metal/ceramic composites for high temperature applications and funded by Swedish Foundation of Strategic Research (SSF). I am extremely thankful for being part of this project.

I would like to extend by deepest gratitude to my supervisor Farid Akhtar for giving me the opportunity to work in this project and for being a source of motivation towards innovative research work. I would also like to thank my co-supervisor Marta-Lena Antti for her fruitful feedback and supervision during the last two years.

I would like to thank Lars Frisk and Johnny Grahn for their tireless effort in helping out in different labs, and for always bringing laughter and positive work atmosphere in the department.

To all my colleagues at the Division of Materials Science, I am extremely grateful for a very good and positive working environment. I would specially like to thank Alberto Vomiero for collaborating with me on thin film synthesis and giving valuable feedback to my work. I would like to thank Mojtaba Gilzad for great talks on life and research, and helping me out with developing new coatings. Many thanks to Magnus Neiktar, Daniel Hedman, Kamran Saeidi, Pedram Ghamgosar and Federica Rigoni for their collaboration in different research work and feedback. I am also grateful for fruitful discussion and help from Hanzhu Zhang, Kritika Narang, Zhejian Cao and Viktor Sandell. I am thankful to my master students Oriol Artola and Anton Ek for helping me out with experimental work on different projects.

Lastly, I would like to thank my parents and brother for their continuous support throughout my life and their unconditional love.

List of Papers

For this thesis, the following papers have been included:

I. Sajid Alvi, Farid Akhtar *"High temperature tribology of CuMoTaWV high entropy alloy"* Wear. 426 (2019) 412-419.

II. Sajid Alvi, Dariusz Jarzabek, Mojtaba Gilzad Kohan, Daniel Hedman, Marta Maria Natile, Alberto Vomiero, Farid Akhtar *"Synthesis and mechanical characterization of CuMoTaWV high entropy film by magnetron sputtering"* (Submitted to ACS Applied Materials & Interfaces).

List of papers not included in this thesis:

I. Sajid Ali Alvi, Farid Akhtar *"High temperature tribology of polymer derived ceramic composite coatings"* Scientific reports. 8 (2018) 15105.

II. Kamran Saeidi, Sajid Ali Alvi, Frantisek Lofaj, Valeri Ivanov Petkov, Farid Akhtar *"Advanced Mechanical Strength in Post Heat Treated SLM 2507 at Room and High Temperature Promoted by Hard/Ductile Sigma Precipitates"* Metals. 9 (2019) 199.

III. Sajid Ali Alvi, Pedram Ghamgosar, Federica Rigoni, Alberto Vomiero, and Farid Akhtar *"Adaptive nanolaminate coating by atomic layer deposition"* (Submitted to Solid Thin Films).

IV. Sajid Ali Alvi, Kamran Saeidi, Farid Akhtar *"High temperature tribology of selective laser melted 316L stainless steel"* (Submitted to Wear).

Table of Contents

1. Introduction

1.1. Aims of this project

The forefront of research in materials science has been developing new materials with good strength and stiffness at higher temperatures for applications, such as aerospace and jet engine. Recently, development of high entropy alloys has made it possible to achieve superior mechanical properties at high temperatures compared to conventional alloys. However, less attention has been given to the tribological properties of high entropy alloys and films. The aim of this licentiate work is to develop refractory high entropy alloy (RHEA) using spark plasma sintering (SPS) and understand the effect of microstructural characteristics on the high temperature tribological properties. The second aim is to develop refractory high entropy films (RHEF) using magnetron sputtering with a single partially sintered target and study the effect of a single target on nanocrystallinity and mechanical properties. Keeping these aims in mind, we have developed a CuMoTaWV RHEA using SPS and studied its high temperature tribological properties up to 600 ^{o}C. Secondly, a single partially sintered target by SPS has been used to develop CuMoTaWV RHEF and its mechanical properties, such as hardness, nano-pillar compression and room temperature tribological studies have been investigated.

1.2. Research questions

The following research questions have been addressed in this thesis:

- What are the microstructural characteristics of RHEA after SPS and its affect on the tribological properties? Secondly, how does the selection of different elements effects the properties at high temperature?
- How does the use of single partially sintered target effects the nanocrystallinity and mechanical properties, such as hardness, tribology and nano-pillar compression in RHEF?

2. Introduction to High entropy alloys

In the past, alloy design has consisted of combining single principal element with minor alloying elements to enhance the mechanical, chemical and/or structural properties. The first work on developing an alloy with multi principle elements was first reported in 2003 by Yeh et al. [1], Cantor et al. [2], and Ranganathan et al. [3] and showed superior properties to conventional alloys, leading to wide spread popularity of multicomponent alloys as high entropy alloys (HEAs) among researchers around the world.

HEAs are defined as alloy system consisting of five or more principal elements with a concentration of each principal element between 35 and 5 at.%. The mixing of multiple components results in high entropy of mixing, expressed by [4,5]:

$$\Delta S_{mix} = -R \sum_{i=1}^{n} c_i \ln c_i \quad \text{(i)}$$

Where, R is the gas constant, c_i the molar fraction of i^{th} element, and n the total number of constituent elements. The configurational entropy has the highest contribution to the entropy of mixing of high entropy alloys as compare to other sources, such as vibrational, electronic and magnetic entropy [6]. For an equiatomic HEA, the entropy would reach a maximum with the configurational entropy (ΔS_{conf}) expressed by:

$$\Delta S_{conf} = R \ln n \quad \text{(ii)}$$

where n is the no of elements. As a result, the ΔS_{conf} for an equimolar alloy with 3, 5, 6, and 9 elements will result in to 1.10R, 1.61R, 1.79R and 2.20R, respectively. Thus, in order for a multicomponent alloy to be classified as HEA, the lower limit of ΔS_{conf} has been suggested to be 1.5R.

The increase in entropy of mixing in multicomponent alloy results in decreasing the Gibbs free energy of mixing (ΔG_{mix}) leading to formation of stable solid solution of face-centered cubic (FCC),

body-centered cubic (BCC) or hexagonal close pack (HCP) crystal structures. The relation between ΔS_{mix} and ΔG_{mix} can be given by the equation (iii) [7]:

$$\Delta G_{mix} = \Delta H_{mix} - T\Delta S_{mix} \quad \text{(iii)}$$

Where ΔH_{mix} is enthalpy of mixing and T is the absolute temperature. The phase formation is determined by the competition between ΔH_{mix} and $T\Delta S_{mix}$. With increasing temperature, a higher $T\Delta S_{mix}$ term becomes more dominant and will lead to formation of solid solution.

2.1. The core effects

The composition of HEAs from five or more principal elements are complex as compare to conventional alloys. Yeh [8] suggested four core effects that describe the properties of HEAs: (1) high entropy effects, (2) sluggish diffusion, (3) severe lattice distortion, and (4) cocktail effects.

2.1.1. High-entropy effect

The high-entropy effect was first proposed by Yeh, which described the stabilization of high-entropy phases with the formation of solid solution phases. According to Gibbs phase rule, the number of phases (P) in a given alloy at constant pressure in equilibrium condition can be expressed as:

$$P = C + 1 - F \quad \text{(iv)}$$

where, C is the number of component and F is the maximum number of thermodynamic degrees of freedom in the system. For example, in a 6-component system at a given pressure, it is expected to have 7 phases at any given reaction. However, compositions satisfying the HEAs-formation criteria will form solid-solution phases [2,9,10].

According to the classical physical-metallurgy theory, a solid solution phase is based on one element (solvent) and contains other minor elements (solutes). However, in HEAs, it is difficult to

differentiate between solvent and solute because of their equimolar compositions. According to many researchers, HEAs can only form simple FCC or BCC solid solution, and the number of phases formed are much smaller than what Gibbs phase rule in equation (iv) allows [8,11]. Thus, indicating that high entropy of alloys expands the solubility limit between chemically compatible elements. This phenomenon can be explained with reference to equation (iii), where the mixing entropy competes with the mixing enthalpy. Furthermore, the $T\Delta S_{mix}$ term becomes more dominant at high temperatures, resulting in minimizing the free energy and forming simple multi-element solid-solution phases.

2.1.2. Lattice distortion effect

In HEAs, each element has the same possibility of occupying a lattice site, and since the size of each element can be different in many cases, this can lead to formation of severed lattice distortion. Furthermore, such lattices with many principal elements are highly distorted, as all the atoms are solute atoms with different atomic sizes, as shown in Figure 2.1. Such severe lattice distortion can lead to higher strength and hardness of HEAs [12]. Yeh et al. [13] also proved the lattice distortion in HEAs by studying its effect on decreasing trend in X-ray diffraction (XRD) intensities of CuNiAlCoCrFeSi alloy system with systematic addition of principal elements.

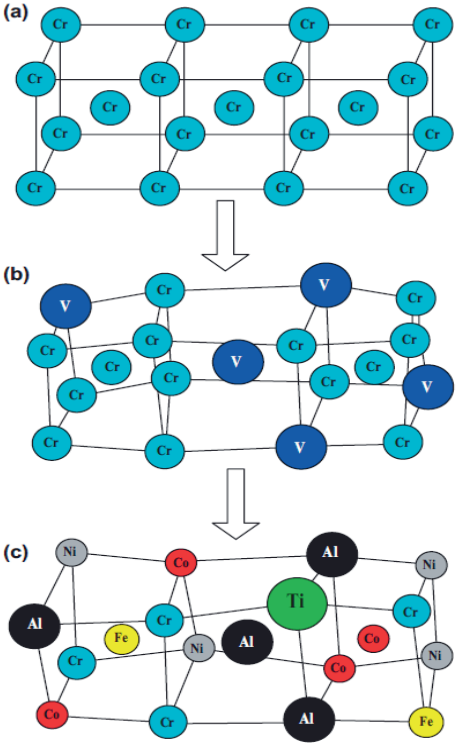

Figure 2.1: Schematic illustration of BCC crystal structure: (a) perfect lattice of Cr; (b) distorted lattice with the addition of V (for example: Cr-V solid solution); (c) extremely distorted lattice caused of atoms with different atomic sizes randomly distributed in the crystal lattice with same probability to occupy the lattice position in HEA system ($AlCoCrFeNiTi_{0.5}$[14]) [10].

2.1.3. Sluggish diffusion

The equilibrium partitioning among the phases is attained through phase transformations that depend on atomic diffusion. However, according to Yeh [8], diffusion in HEAs are hindered due to lattice distortion, thus limiting the diffusion rate. During the conventional casting of HEAs, the phase separation during cooling is inhibited at a higher temperature and the resulting alloy has nano-precipitates in the matrix. Such formation of nano-precipitates in HEAs results in higher recrystallization temperature and activation energies during deformation. The sluggish diffusion

in coatings, such as by magnetron sputtering, results in the formation of nanocrystalline or amorphous phase for a higher number of principal element as the growth and nucleation of crystalline phases are inhibited, as shown in Figure 2.2 [15]. Such structural variation with a different number of principal elements can be easily exploited in HEAs to promote the mechanical, physical and chemical properties.

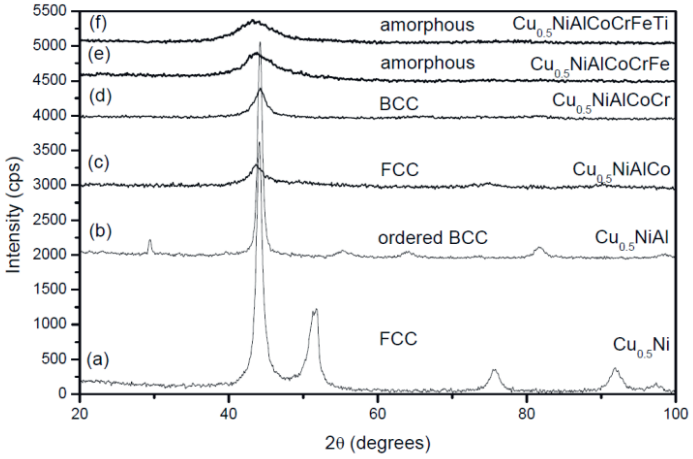

Figure 2.2: XRD analysis showing structural evolution of two to seven elements sputtered films [15].

2.1.4. Cocktail effect

According to Yeh [8], the incorporation of multi-principle elements in HEAs can be considered as an atomic-scale composite. This composite effect is characterized by the basic features and interactions between all the elements present in HEA along with the indirect effects of different elements on the microstructure. Thus, the term cocktail effect, first mentioned by Ranganathan [3], comes from the properties resulting from combination of principal elements that cannot be obtained from only a single principle element. For example, light elements are selected for developing a HEA with lighter density, such as Al, Cr Cr, Cu, Fe, Ni and Si. For oxidation resistance at higher temperatures, Si, Al and Cr are used [16]. To increase the strength, Al is added to a multi-element

system of Co, Cr, Cu, Fe and Ni, which promotes the formation of BCC along with inducing higher strength, as shown in Figure 2.3 [17,18].

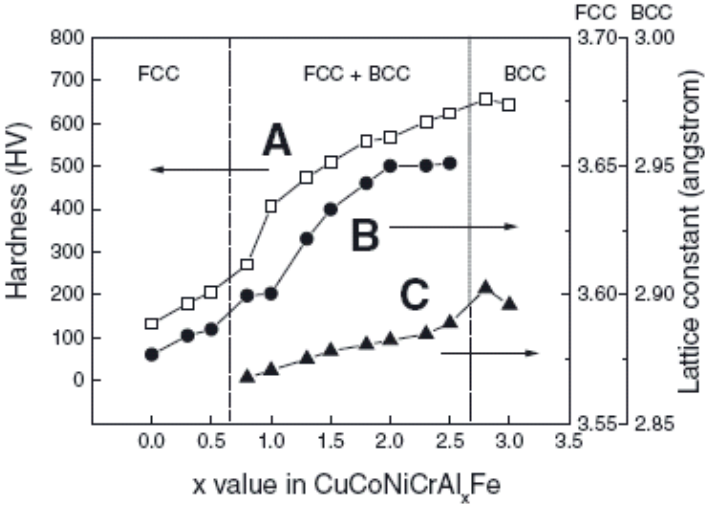

Figure 2.3: Effect of aluminum addition on the cast hardness of Al_xCuCoNiCrFe alloys. A, B and C refers to that hardness, FCC lattice constant and BCC lattice constant, respectively [8].

2.2. Alloy preparation

2.2.1. Arc Melting (Liquid state)

The most widely used processing technique for HEAs development is arc melting technique. The typical schematic of arc melting method is shown in Figure 2.4. The electrode temperature of arc melting furnace can go in excess of 3000 ^{o}C, which can be controlled by adjusting the electrical power. Thus, arc melting technique is beneficial towards homogenous melt mixing of elements with high melting points, such as refractory elements. However, heterogeneous microstructure (dendritic with interdendritic segregation) in the resulting HEAs are induced by the thermal gradient from surface to center during solidification, which makes the microstructure and properties of as-cast HEAs less controllable. Furthermore, large differences in elemental

melting temperatures can result in elemental segregation in refractory HEAs casted from liquid state [19,20]. The use of arc melting technique restricts the as-casted alloy shapes to rods and buttons, thus complex shapes are difficult to cast for advanced applications.

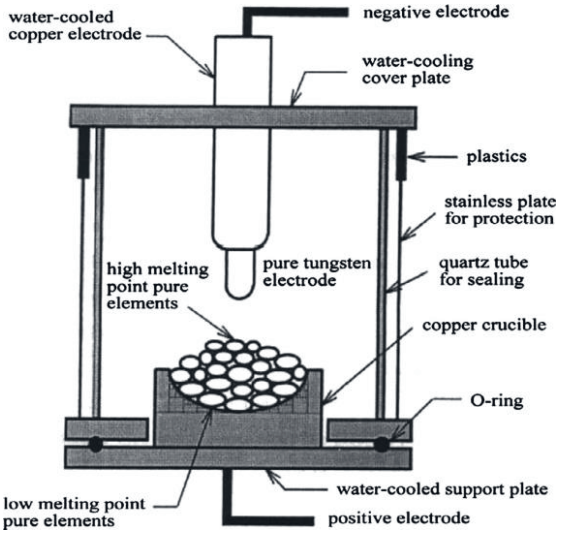

Figure 2.4: A schematic representation of the arc melting process [21].

2.2.2. Spark plasma sintering (Solid state)

Mechanical alloying (MA) is a process consisting of high-energy ball milling of elemental powders at room temperature for a long duration of time resulting in diffusion of species into each other to obtain homogenous alloy. Murty's research group was the first to demonstrate the use of MA to synthesize nanostructured equiatomic AlFeToCrZnCu HEA, where each nanoparticle obtained was equiatomic in its composition [22].

The HEAs developed by MA are in powder form and needs sintering in order to get a dense component. In order to avoid grain growth of nanocrystalline alloy powder during conventional sintering process, spark plasma sintering (SPS), also known as pulsed current processing (PCP), is used to obtain nanocrystalline

alloys. SPS employs the usage of high amperage pulse current of up to 5000 A with simultaneously applying uniaxial pressure of up to 100 MPa through powder mixture packed in a graphite die, as shown in Figure 2.5. Graphite paper is usually added between the sample and the graphite die to avoid unnecessary reaction of the powder mixture with the die. The combination of high current pulse, uniaxial pressure and vacuum/inert atmosphere leads to consolidation of powders at very short time.

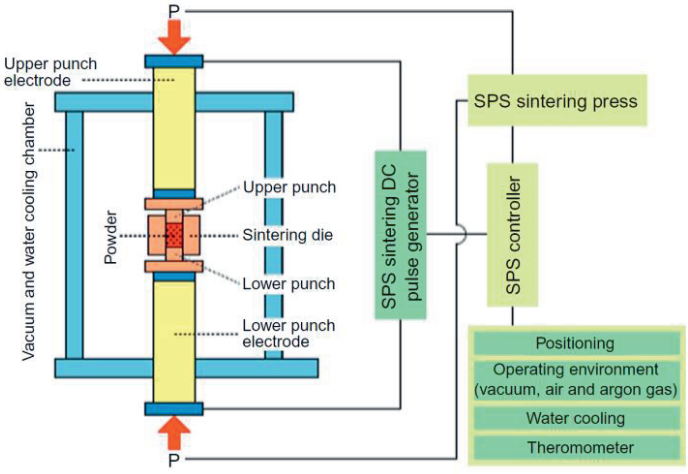

Figure 2.5: Schematic of spark plasma sintering [23].

Compared to conventional liquid state alloy development of HEA, such as arc melting, SPS has been used to develop nanocrystalline HEAs [24–26]. Recently, researchers have employed SPS to develop composite HEAs for tribological applications. Zhang et al. [27] developed CoCrFeNi-Ag-BaF_2/CaF_2 composite HEA and showed low frictional (COF: 0.2 to 0.25) and wear (wear rate: 2 x 10^{-5} mm^3/Nm to 5 x 10^{-5} mm^3/Nm) behavior against Inconel 718 counter balls from RT to 800 ^oC. Similarly, Cao et al. [28] developed NiCoCrAl-Ag-MoS_2-LaF_3-CeF_3 composite HEA using SPS and studied the high temperature tribology from RT to 800 ^oC against Si_3N_4 balls, and showed adaptive frictional (COF: 0.3-0.4) and wear behavior (wear rate: 2.05 x 10^{-5} mm^3/Nm to 5.18 x 10^{-6} mm^3/Nm).

2.2.3. Magnetron sputtering (Gaseous phase)

Magnetron sputtering is a type of physical vapor deposition (PVD) technique that is used for deposition of thin films on a substrate through sputtering away atoms from target material (elemental or alloy) under the bombardment of charge Ar^+ ions. Simple schematics of sputtering process is shown in Figure 2.6. There are two types of sputtering techniques commonly used: direct current (DC) sputtering and radio frequency (RF) sputtering. DC sputtering is a technique where DC bias is applied between the target and substrate to deposit the atoms generated from the target material. Controlling power, bias voltage, and the argon pressure controls the deposition rate of film onto the substrate. The second type of sputtering (RF sputtering) is used for deposition of insulating materials, where plasma can be maintained even at lower argon pressure resulting in fewer gas collisions and line of sight deposition [29].

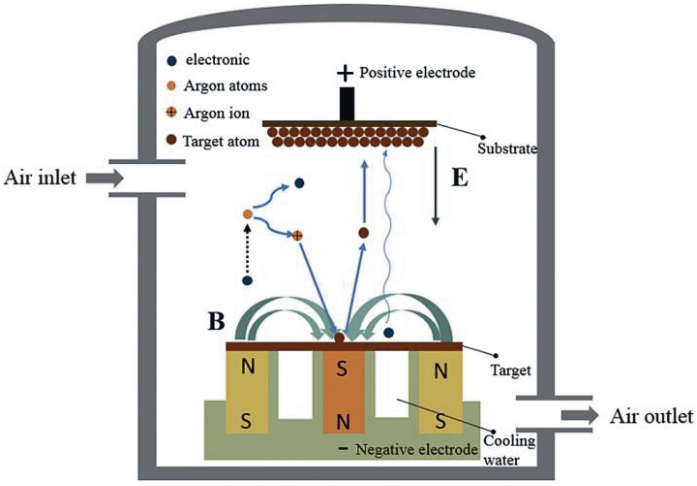

Figure 2.6: Schematic of magnetron sputtering deposition process [30].

Many researchers have explored magnetron sputtering technique in the last decade to develop thin films of high entropy alloy, high entropy nitride and high entropy carbides [31]. The major advantage of using magnetron sputtering for developing high

entropy film is the control of reactive gases (such as N_2, O_2 or CH_4/C_2H_2) [32–36], nanocrystallinity [37] and influence of deposition condition (such as substrate temperature and substrate bias) [38–40]. Such control on different parameters results is obtaining high entropy films with superior properties, such as high hardness [32,41–43], high compressive strength [44–46], corrosion resistance [39,47], wear resistance [36,48–51], unique physical characteristics [52–54] and high temperature stability [48,55,56].

2.3. Refractory high entropy alloys

Refractory metals consisting of W, Mo, Ta and Nb, and its alloys are critical for applications that require high temperature strength due to their high temperature melting point (T_m). The definition of refractory metals also extends to include Ti, Zr, Hf, V, Re, Ru, Os and Ir. Some of the key properties, such as melting point, density and crystal structure, of refractory metals are listed in Table 2.1. Among the refractory metals, Ti is the lightest element with a density of 4.507 g/cm^3 while Ir is the heaviest with a density of 22.65 g/cm^3.

The initial research on HEAs was focused on 3-d transition metal (TM) of Co, Cr, Cu, Fe, Mn, Ni, Ti, and V [57]. However, to develop HEA for high temperature applications, TM HEAs fail to operate above 600 ^oC [58]. Following the founding motivation, Senkov et al. in 2010 first reported the development of refractory high entropy alloys (RHEAs) based on five refractory elements of Mo, Nb, Ta, V, and W that showed superior high temperature (above 1000 ^oC) mechanical properties [19,59]. Subsequently, different researchers incorporated other refractory elements from Group IV (Ti, Zr, and Hf), Group V (V, Nb, and Ta), and group VI (Cr, Mo, and W) to further increase the mechanical properties of RHEAs at wide temperature ranges [58]. RHEA tend to form a BCC crystal structure and may also contain Laves phases if Cr or V are also present in the alloy. The densities of RHEA can range from 5.6 to 13.7 g/cm^3, which is higher than TM HEAs with

densities ranging from 5.0 to 9.0 g/cm^3. Thus, small amounts of non-refractory elements, such as Al, Si, Co or Ni, are added to lower the density or increase the ductility of RHEA at room temperature [60].

Table 2.1: Melting point, density and crystal structure of different refractory elements [61].

Element	Melting point (°C)	ρ (g/cm^3)	Crystal Structure
Titanium (Ti)	1668	4.507	Polymorphic (HCP/BCC)
Zirconium (Zr)	1855	6.511	Polymorphic (HCP/BCC)
Hafnium (Hf)	2233	13.31	Polymorphic (HCP/BCC)
Vanadium (V)	1910	6.11	BCC
Niobium (Nb)	2477	8.57	BCC
Tantalum (Ta)	3017	16.65	BCC
Chromium (Cr)	1907	7.14	BCC
Molybdenum (Mo)	2623	10.28	BCC
Tungsten (W)	3422	19.25	BCC
Rhenium (Re)	3186	21.06	HCP
Ruthenium (Ru)	2334	12.37	HCP
Osmium (Os)	3033	22.61	HCP
Rhodium (Rh)	1964	12.45	FCC
Iridium (Ir)	2466	22.65	FCC

RHEAs are mostly developed using arc melting technique. However, arc melting can lead to typical solidification defects, such as elemental segregation, micro-/macro-segregation, pores and residual stresses due to large differences in elemental melting

temperatures [19,20]. Recently, SPS has been employed to develop dense and fine-grained RHEA from elemental or pre-alloyed powders [26][62].

2.3.1. Properties

2.3.1.1.Mechanical

RHEAs are considered as future alloys for high temperature application to replace the current Ni-based super-alloys due to their high mechanical properties at different temperature ranges, as shown in Figure 2.7 [63]. Therefore, there is a great research effort to identify alloy compositions that have good overall strength and ductility from RT to high temperatures (above 1000 ^{o}C) [58]. The first reported RHEA of MoNbTaW and MoNbTaWV showed high compressive yield strength of 421-506 MPa and 656-735 MPa, respectively, in the temperature range of 1400-1600 ^{o}C [59]. Similarly, most of the RHEA reported have been found to have good mechanical properties at temperatures higher than 600-800 ^{o}C. However, it was found to be brittle at RT due to interstitial elements segregating to grain boundaries during solidification or annealing. Addition of Group IV elements, such as Hf, Ti and Zr, generally enhances the ductility, and addition of Group V and VI elements and/or Al increases the strength of the materials but promotes low ductility. Consequently, new RHEAs, such as addition of Ti in MoNbTaW and MoNbTaWV, were designed to increase the RT ductility while maintaining high compressive strength at a broad range of temperatures [64,65]. Recently, researchers have developed RHEAs with the addition of carbon and Si to prepare RHEA with the formation of MC carbides (M: Hf, Nb, Ti, or Zr) and M_5Si_3 phases, respectively [66–69]. The formation of carbides was found to increase the ductility and work hardening at RT for low carbon content, such as $C_{0.1}Hf_{0.5}Mo_{0.5}NbTiZr$ [67]. In another work by Guo et al., the effect of adding small amounts of Si (~2.5 at.%) in $Hf_{0.5}Mo_{0.5}NbTiZr$ to form M_5Si_3, which resulted in grain refinement and improved compressional strength and ductility

[66]. Another strategy for RHEA seeks to develop light-weight RHEA by reducing the density while keeping superior mechanical properties using Cr, Nb, Mo, Ti, V, and Zr as principal elements, such as Al_xTiVZr_y alloys, reducing the densities to 5.6-5.7 g/cm^3 [70,71]. Similarly, Senkov et al. developed a light-weight RHEA of CrNbTiVZr with a density of 6.57 g/cm^3 and had a yield strength of 187 MPa and 94 MPa at 600 ^oC and 800 ^oC, respectively [60,72].

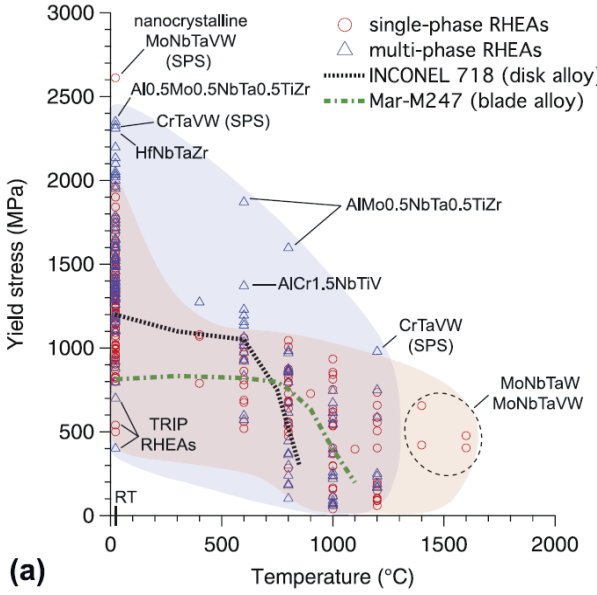

Figure 2.7: Comparison of yield stress variation at different temperatures of different RHEAs with two Ni-base superalloys Inconel 718 and Mar-M247 [58]. RT: room temperature; SPS: spark plasma sintering; TRIP: transformation-induced plasticity.

Recently, RHEAs of $HfNb_{0.18}Ta_{0.18}Ti_{1.27}Zr$ and $Ta_{0.4}HfZrTi$ have been developed to improve the work hardening and tensile ductility through deformation-induced phase transformations, also known as transformation induced plasticity (TRIP) [73,74]. This strategy resulted in yield stress of 400-500 MPa through forming strain-localized regions of HCP phase in $Ta_{0.4}HfZrTi$ and α'' martensite in $HfNb_{0.18}Ta_{0.18}Ti_{1.27}Zr$.

2.3.1.2.Tribological behavior

The tribological studies of RHEA are scarce. Poulia et al. [75] studied the dry sliding wear behavior of MoTaWNbV RHEA (7576 $HV_{0.5}$) developed by arc-melting against alumina and steel counter-balls at RT and compared its wear behavior with Inconel 718. The wear rate of MoTaWNbV RHEA was found to be 1.57 x 10^{-4} mm^3/Nm and 2.3 x 10^{-4} mm^3/Nm against alumina and steel counter-ball, respectively. In contrast, Inconel 718 had a higher wear rate of 4.57 x 10^{-4} mm^3/Nm and 8.3 x 10^{-4} mm^3/Nm against alumina and steel counter-ball, respectively. In subsequent work, Mathiou et al. [76] studied the dry sliding wear of MoTaNbZrTi against alumina and steel counter-ball at RT with different sliding distances and compared it to MoTaNbWV RHEA. The wear rate of MoTaNbZrTi with sliding distance from 400 m to 2000 m was reported to have decreasing trend from 0.199 x 10^{-4} mm^3/Nm to 0.141 x 10^{-4} mm^3/Nm against steel counter-ball, and an increasing trend from 1.13 x 10^{-4} mm^3/Nm to 1.41 x 10^{-4} mm^3/Nm against alumina counter-ball. In all tribological test conditions, the wear rate of MoTaNbZrTi RHEA was found to be lower than MoTaNbWV RHEA. However, there is still a research gap is studying the high temperature tribological behavior of RHEA.

2.4. Refractory high entropy films

In the last 5 years, there have been few research work reported on refractory high entropy films (RHEFs) by magnetron sputtering. Although, more work has been done on nitrides of RHEFs [51,77,78]. Majority of the research on RHEFs has been reported on NbMoTaW composition [37,44,45,79,80], along with few studies on HfNbTiVZr [38] and TiTaHfNbZr [81] compositions.

2.4.1. Properties

2.4.1.1.Mechanical

RHEFs developed using magnetron sputtering leads to the formation of nanocrystalline grains, which in return enhances the

mechanical properties, such as hardness and nano-pillar compressional strength. Zou et al. [44,45] studied the nanocrystalline (nc) pillar compression of NbMoTaW RHEF from RT to 600 ^{o}C, and reported high compressional strength up to 10 GPa (RT) and 5 GPa (600 ^{o}C). It was reported that with the decrease in nc-pillar diameter, the highest compressional strength of 10 GPa was obtained at ~70-100 nm, and were found to be higher than all the reported nc-metals in the literature [82]. Furthermore, even after annealing of NbMoTaW RHEF at 1,100 ^{o}C for 3 days, the film retained its needle-like morphology and nc-pillar compressional strength. The Ashby inspired map of specific strength versus test temperature of pillar compression of different metals and alloys are shown in Figure 2.8 [45]. Furthermore, even after annealing of NbMoTaW RHEF at 1,100 ^{o}C for 3 days, the film retained its needle-like morphology and nc-pillar compressional strength.

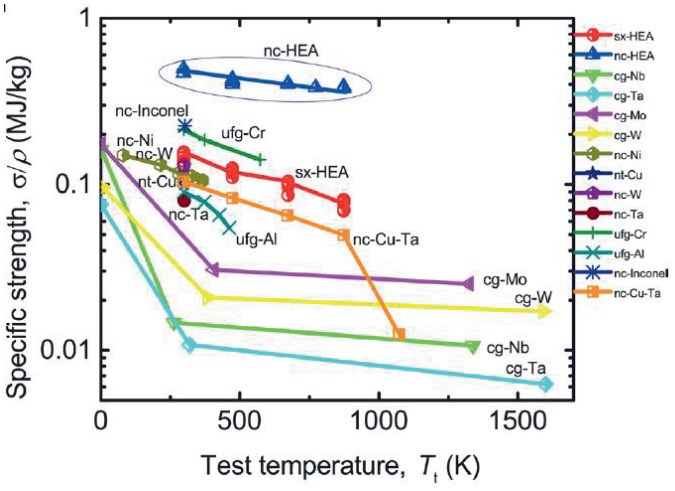

Figure 2.8: Ashby inspired specific strength versus temperature plot of pillar compression of different nc-metals, showing that nc-HEA exhibit the highest strength-to-density ratio at different temperatures [45].

Feng et al. [79] studied the effect of film thickness on mechanical properties of NbMoTaW RHEF using nanoindentation technique. It was reported that with the increasing film thickness (100 nm to

2000 nm), nanoindentation hardness and elastic modulus decreased from ~16 GPa and ~200 GPa to ~11 GPa and ~185 GPa, receptively. This decrease in mechanical properties was attributed to the grain coarsening as the grain size increased from 10 nm to ~32 nm with increasing film thickness. Similarly, Kim et al. [37] studied the effect of using single alloyed target sputtering versus the use of elemental co-sputtering of the target on the nanocrystallinity and mechanical properties of NbMoTaW RHEF. A partially sintered alloy target of NbMoTaW was developed using hot pressing followed by sintering at 1400 ^{o}C. The mean grain size of deposited NbMoTaW RHEF was found to be 15.8 nm, whereas Zou et al. [44] reported a grain size of 150 nm of same composition using elemental co-sputtering from multiple targets. Fritze et al. [38] studied the influence of deposition/substrate temperature on the phase evolution and mechanical properties of HfNbTiVZr RHEF. With the increase in substrate temperature from RT to 450 ^{o}C, a transition from amorphous phase to BCC matrix with C14 or C15 Laves phase precipitates were observed. Furthermore, the nanoindentation hardness also increased from 6.5 GPa to 9.2 GPa with increasing substrate temperature.

2.4.1.2.Tribological behavior

Tuten et al. [81] reported on tribological studies of TiTaHfNbZr RHEF deposited on Ti-6Al-4V alloy substrate using RF magnetron sputtering technique for biomedical applications. The resulting RHEF showed an average hardness and Young's modulus of 12.51 GPa and 181 GPa, respectively. The sliding test against alumina counter-ball showed low frictional coefficient from 0.1 to 0.2 with increasing normal load from 1 to 3N. The low frictional coefficient has been attributed to the nanocrystallinity of RHEF. There is still a research gap for tribological studies of RHEF, which needs to be fulfilled in the coming future, especially at higher temperatures.

2.5. Existing research gaps

Although the research on refractory high entropy alloys (RHEA) and refractory high entropy films (RHEFs) is rather new, many researchers have reported its mechanical (hardness/tensile/compression/creep) performance at wide temperature ranges as alternate to Ni-based super alloys. However, the work on high temperature tribological studies of RHEAs and RHEFs has received less attention. The underlying mechanism of wear at different temperatures also needs further investigation in relation to microstructure and crystallographic orientation of RHEAs and RHEAFs. Furthermore, the selection of different principle element's effect on the tribological properties of RHEA and RHEF at different temperature ranges needs to be investigated. Thus, keeping this research gap in mind, this thesis tries to cover the high temperature wear mechanism in CuMoTaWV RHEA and RT tribological behavior in CuMoTaWV RHEF.

3. Experimental methods

3.1. Spark plasma sintering (SPS)

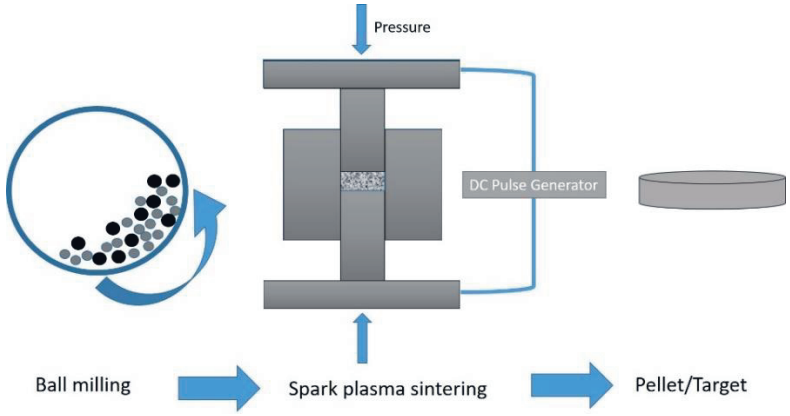

Figure 3.1: Schematic of alloy development from powder mixture to sintering using SPS.

Equimolar mixture of Cu, Mo, Ta, W and V powders were fed into a plastic vial and mixed for one hour using ball milling. Alumina balls were used for ball milling process with a ball to powder ratio of 3:1. Details of the starting powders are shown in Table 3.1. Nano powder of W was used in paper I due to its low diffusion coefficient. The resulting powder mixture was fed into graphite die with a diameter of 12 mm and 76 mm for paper I and paper II, respectively. The SPS in paper I was carried out in ultrahigh vacuum environment using SPS 825 (Dr. Sinter Spark Plasma Sintering System), and SPS in paper II was used under argon atmosphere using SPS 530ET (Dr. Sinter Spark Plasma Sintering System) to consolidate powder mixture for target development. A heating rate of 50 ^{o}C/min and holding time of 10 mins was used in paper I, while a heating rate of 100 ^{o}C/min was used for target development in paper II. The details of heating rate

and holding time parameters for both papers are shown in Figure 3.2.

Table 3.1: Particle size distribution of starting material in paper I and paper II

	Cu	Mo	Ta	W	V
Paper I	10 µm	3-7 µm	44 µm	70 nm	44 µm
Paper II	10 µm	3-7 µm	44 µm	44 µm	44 µm

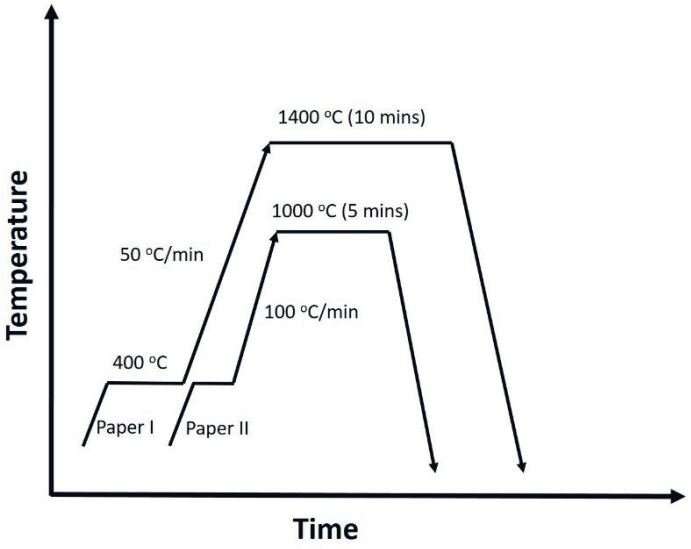

Figure 3.2: Schematic of heating cycles for SPS in paper I and paper II.

3.2. Magnetron sputtering

An equimolar CuMoTaWV target for sputtering deposition with a diameter of 76 mm and a thickness of 3 mm was developed using SPS 530ET (Dr. Sinter Spark Plasma Sintering System), as shown in Figure 3.3. Direct current (DC) magnetron sputtering (Moorfield, UK) was used to deposit CuMoTaWV RHEF on silicon and 304 stainless steel substrate in paper II.

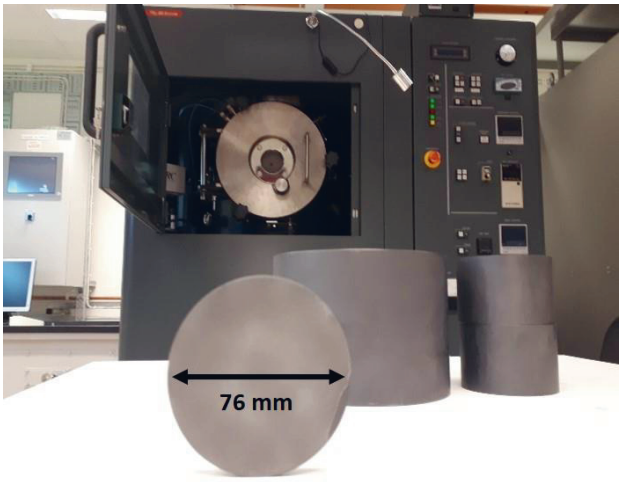

Figure 3.3: Target prepared at 1000 ^{o}C using SPS.

The RHEF was deposited on silicon substrate for cross-section analysis, nanoindentation hardness measurement, nano-pillar compression test, Rutherford backscattering analysis (RBS) and X-ray photoelectron spectra (XPS) analysis; and on 304 stainless steel substrate for XRD analysis and tribological tests. Sheet metal substrate of 304 stainless steel with a thickness of 5 mm was cut into 20 x 20 mm and diamond polished up to 0.4 µm, followed by cleaning with ethanol in ultrasonicator for 30 mins and dried in an oven at 80 ^{o}C for 30 mins. Silicon substrate with a thickness of 2 mm and dimensions of 5 x 5 mm were used after rinsing with ethanol and distilled water followed by drying in an oven at 70 ^{o}C. The parameters for film deposition, as shown in Table 3.2, were used to get a film thickness of ~900 nm. A substrate temperature of 500 ^{o}C was used to enhance the sputtering yield.

Table 3.2: Sputtering parameters for deposition of CuMoTaWV high entropy film	
Substrate temperature (^{o}C)	500
Atmosphere	Ar
Gas Flow (sccm)	20
Substrate rotation speed (rpm)	7
Deposition pressure (mPa)	1.16×10^{-3}
Deposition power (W)	150
Deposition duration (min)	120
Deposition rate (nm/min)	7.5

3.3. Microhardness measurement

In paper I, microhardness measurements were performed using Vickers microhardness (Matsuzawa, MXT-CX) equipped with diamond indenter at 200 g load. The samples were diamond polished up to 0.4 µm to get a smooth surface for hardness measurement. At least 8 indentations were performed at different location of interest.

3.4. Nanoindentation

In paper II, hardness measurements were performed using nanoindenter (Micro Materials, UK) at 10 mN load. The nanoindentation tests were performed at loading, unloading and duel time of 25 sec, 20 sec and 10 sec, respectively. Nanoindentation measurements were performed to obtain force-displacement curve at 12 different location and the average hardness and Young's modulus were reported in the paper.

3.5. Nano-pillar compression tests

In paper II, nano-pillars were developed in CuMoTaWV RHEF using focused-ion beam (FIB) for compression tests. For each pillars, firstly, a ring was etched using high current (1 nA) with the outer and inner diameter set to 30 µm and 8 µm, respectively. Lastly, fine etching of a pillar with current lower than 320 pA was used to mill 440 nm diameter pillars. The pillars were then compressed using Anton Paar ultra-nanoindentation tester in

the load control mode with a maximum force set to 3 mN using a flat punch with a diameter of 20 µm. The loading and unloading rates were set to 1 mN/min and 3 mN/min, respectively. The data acquisition rate was set to 50 Hz. The value of the compression strength was determined as the engineering strain at which 0.2% plastic deformation occurs. Young's modulus was determined from the linear fit to the data for which engineering stress was lower than 0.6 compression strength. Engineering stress was determined by dividing the force measured by nanoindentation tester over pillars cross-section area. Hence, we have measured the pillars diameters before and after the compression test with the use of SEM. Furthermore, in order to determine engineering strain, the ratio of displacement obtained from nanoindentation to the initial height of a pillar measured by atomic force microscope (AFM) was obtained.

3.6. Tribological studies

Tribological tests in paper I and paper II were carried out using universal tribometer (Rtec Instruments, San Jose, USA) equipped with a normal load (Fn) sensor in the range of 1-100 N and frictional force (Fx) sensor in the range of 1-50 N.

High temperature tribology

For paper 1, high temperature furnace with asbestos lining was used to perform high temperature tribological tests. A ball-on-disc sliding tests were performed on CuMoTaWV RHEA with dimensions of 12 mm diameter and 5 mm thickness. The tribological tests were performed at room temperature (RT), 200 ^{o}C, 400 ^{o}C and 600 ^{o}C for sliding distance of 200 m. The tribological tests were performed against Si_3N_4 counter-ball with a diameter of 9.5 mm. The counter-ball was washed in ethanol and distilled water in ultrasonic machine followed by drying in oven at 70 ^{o}C. A normal load of 5 N was applied in all test. The counter-ball and specimen was brought in contact after the desired test temperature was reached. For repeatability of the tribotests, three tests/condition were conducted and the average COF and wear rate

were reported. The average depth of the resulting wear track was measured using optical profilometry (Wyko) to calculate the specific wear rate at each temperature. At least 8 wear track depth was measured for each tribotest. The wear rate, expressed as mm^3/Nm, was measured by dividing wear volume with normal load and sliding distance.

Room temperature tribotest

For paper II, RT tribotest of CuMoTaWV RHEF was performed in the ball-on-disc setup at 1 N normal load and a sliding speed of 0.1 m/s. A counter-ball of E52100 alloy steel (Grade 25, 700-880 HV) with a diameter of 6.3 mm was used after cleaning with ethanol in a ultrasonicator machine for 10 mins followed by drying in an oven at 80 ^oC for 30 mins. The average depth of wear was measured using optical profilometry (Wyko) to calculate the wear rate expressed in mm^3/Nm.

3.7. Scanning electron microscopy (SEM)

SEM analysis was performed using JSM-IT300 (JEOL, Tokyo, Japan) and Magellan 400 XHR-SEM (FEI Company, Eindhoven, Netherlands) based on the requirement of magnification. In paper I, JSM-IT300 was used to characterize the microstructure of CuMoTaWV RHEA and the resulting wear tracks after high temperature tribotests. The accelerating voltage for microstructural analysis and wear track analysis from tribotest was set to 15 kV and 10 kV, respectively.

In paper II, Magellon 400 was used to characterize the coating surface and cross-section morphology of CuMoTaWV RHEF; and JSM-IT300 was used to characterize the wear tracks resulting from tribotests.

3.8. XPS measurements

X-ray photoelectron spectra (XPS) were recorded using a PerkinElmer PHI 5600 ci spectrometer with a standard Al−Kα source (1486.6 eV) working at 250 W. The working pressure was

set to 5×10^{-8} Pa. The spectrometer was calibrated by assuming the binding energy (BE) of the Au 4f7/2 line to be 84.0 eV with respect to the Fermi level. Extended spectra (survey) were collected in the range 0−1300 eV (187.85 eV pass energy, 0.5 eV step, 0.025 $s \cdot step^{-1}$). Detailed spectra were recorded for the following regions: V 2p, Mo 3d, Ta 4f, W 4f, Cu 2p and O1s (23.5 eV pass energy, 0.1 eV step, 0.2 $s \cdot step^{-1}$). The atomic percentage, after a Shirley type background subtraction, was evaluated by using the PHI sensitivity factors. The sample was analyzed before and after 2 min Ar^+ sputtering at 3.5 keV with an argon partial pressure of 5×10^{-8} mbar and a rastered area of 2.5 x 2.5 mm.

3.9. Rutherford backscattering spectrometry

In paper II, Rutherford Backscattering Spectrometry (RBS) with a 1.8 or 2.0 MeV $4He^+$ beam in IBM geometry was used to measure the composition homogeneity in the CuMoTaWV RHEF.

3.10. Atomic force microscopy (AFM)

In paper II, the AFM analysis was used to study the surface morphology and surface roughness of CuMoTaWV RHEF. The AFM measurements were performed using ambient conditions with an NTEGRA AFM (NT-MDT) in semi-contact mode using a polysilicon lever, monocrystal silicon probe (HA_NC series) with a tip height of 10 μm, nominal tip radius less than 10 nm, and a measured resonance frequency of 240.3 Hz.

3.11. DFT calculations

In paper II, density-functional theory (DFT) was applied to predict the lattice structure and mechanical properties of CuMoTaWV RHEF. Based on experimental XRD analysis, DFT calculation was used to compare the theoretical and experimental peak positions (2θ) of different planes.

4. Summary of appended papers

Paper I

Title: High temperature tribology of CuMoTaWV high entropy alloy.

In this work, an equiatomic CuMoTaWV high entropy alloy was developed using spark plasma sintering (SPS) of elemental powder mixture at 1400 ^{o}C. The objective of this paper was to see how the microstructural changes at different temperature effects the tribological properties. The resulting sintered alloy showed formation of BCC solid solution along with V-rich phases with an average hardness of 600 HV and 900 HV, respectively. Room temperature (RT) ball-on-disc sliding wear against alloy steel at 5 N load showed negligible wear rate. Thus, Si_3N_4 as a counter-ball was used against sintered CuMoTaWV high entropy alloy in sliding motion to induce more wear. High temperature tribological studies of the sintered alloy showed wear properties specific to test temperatures. The tribological tests from RT to 600 ^{o}C showed an increasing average COF from RT to 400 ^{o}C and then decreased to at 600 ^{o}C. The wear rate was found to be lower at RT and 400 ^{o}C, and slightly higher at 200 ^{o}C and 600 ^{o}C. The wear surfaces were analyzed to elucidate the wear mechanism at each test temperature. The wear of CuMoTaWV alloy was governed by adhesive wear at RT, adhesive with mild abrasion wear at 200 ^{o}C, and oxidative wear at 400 ^{o}C and 600 ^{o}C. The CuMoTaWV alloy showed adaptive wear behavior at test temperatures of 400 ^{o}C and 600 ^{o}C. At 400 ^{o}C, the adaptive behavior was found to be due to the formation of CuO, resulting in reducing the wear; while at 600 ^{o}C, the transformation of V-rich zones to elongated magneli phases of V_2O_5 reduced the COF to 0.54.

Author's Contribution:

The author planned and performed all the experimental work. The manuscript was written together with the corresponding author.

Paper II

Title: Synthesis and mechanical characterisation of CuMoTaWV refractory high entropy film by magnetron sputtering.

This work involves the development of CuMoTaWV refractory high entropy film (RHEF) using DC-magnetron sputtering. The objective of this work was to see the effect of a single-alloy target on the nanocrystallinity and mechanical properties of thin films. Alloy target of equiatomic CuMoTaWV was partially sintering using SPS process. The developed target was deposited on two different substrates of silicon and 304 stainless steel. The deposited CuMoTaWV RHEF showed formation of BCC solid solution with a lattice parameter of 3.18 Å, which was found to be in good agreement with the one for the DFT optimized SQS (3.16 Å). The film's compositional homogeneity was characterized using Rutherford backscattering (RBS) and showed the presence of Cu and V rich at the coating-substrate interface, while Mo, Ta and W were found to be rich towards the surface of the film. Similarly, XPS analysis of the film after 3 and 4 minutes of etching also showed a high concentration of Mo, Ta and W situated towards the top-surface of the film. The nanohardness measurements were performed using nanoindentation at 10 mN load and showed an average hardness and Young's modulus 19.5 ± 2.3 GPa and 259.3 ± 19.2 GPa, respectively. Nano-pillars from CuMoTaWV RHEF with a diameter of 440 nm were developed using focused-ion beam (FIB) analysis for compressional studies. The nano-pillar compression analysis gave an average compressional strength and Young's modulus of 10.7 ± 0.8 GPa and 196 ± 10 GPa, respectively. Such high hardness and compressional strength are due to the nanocrystallinity and grain boundary strengthening of the films with an average grain size of 18 nm. Tribological performance of CuMoTaWV RHEF deposited on 304 stainless steel was studied against alloy steel at RT. The tribotest showed removal of the film after 15 m of sliding distance. Thus, the film was annealed at 300 ^{o}C to increase the adhesion of film with the substrate. After

annealing, the film showed a steady state COF of 0.25 and a low wear rate of 6.4 x 10^{-6} mm^3/Nm over a sliding distance of 50 m.

Author's Contribution:

The author performed target preparation, coating synthesis, nanoindentation measurements and tribological studies, analyzed all the experimental data. The manuscript was written together with the corresponding author.

5. Conclusions

What are the microstructural characteristics of RHEA after SPS and its effect on the tribological properties? Secondly, how does the selection of different elements effects the properties at high temperature?

The synthesized CuMoTaWV RHEA using SPS showed composite structure with the formation of BCC HEA phase and the presence of hard V-rich phase. The composite structure was obtained due to consolidation of the elemental powder mixture at low temperature of 1400 ^{o}C, which is much lower than the melting point of each refectory element used. The tribological properties showed a low frictional and wear properties at RT due to the presence of hard V-rich phases and formation of tribofilm rich in oxides of W and Ta. Adaptive wear behavior was observed during tribology test at 400 ^{o}C and 600 ^{o}C. The oxidation of Cu at 400 ^{o}C resulted in formation of CuO, which helped in reducing the wear; and the hard V-rich zones transformed to elongated V_2O_5 phase at 600 ^{o}C, which helped in reducing the friction coefficient. This study helped us prove that the microstructure and selection of elements for RHEA is critical for tribological applications at different temperatures.

How does the use of single partially sintered target effects the nanocrystallinity and mechanical properties, such as hardness, tribology and nano-pillar compression in RHEF?

CuMoTaWV RHEF was synthesized with DC-magnetron sputtering using single partially sintered target. The resulting film showed nanocrystalline BCC crystal structure with lattice parameter and grain size of 3.18 Å and 18 nm, respectively. The nanocrystallinity remained stable even after annealing at 300 ^{o}C. The RBS and XPS studies showed that the films have high concentration of Cu and V at the coating-substrate interface while high concentration of Ta, W and Mo was found towards coating

surface. The compositional in-homogeneity can be linked to the higher sputtering of Cu than refractory elements resulting in its lower deposition rate towards the surface of the film. The mechanical properties of RHEF showed an average hardness and nano-pillar compressional strength of 19 ± 2.3 GPa and 10.7 ± 0.8 GPa, respectively. The high hardness and compressional strength of RHEF has been attributed to the combined effect of nanocrystallinity, solid solution strengthening and grain boundary strengthening. The mechanical properties were found to be superior to previously reported RHEF, which used elemental co-sputtering of targets. The RT tribology studies showed low frictional behavior and good adhesion of films after annealing at 300 ^{o}C.

6. Future work

For future work, the objective of doctorate thesis would be twofold:

I. New compositions of RHEA would be synthesized using SPS for high temperature mechanical and tribological applications. Major emphasis of alloy development would be to increase the number of principle elements (up to eight refractory elements) to see if the increase in configurational entropy can stabilize the resulting solid solution and have a single-phase crystal structure. Secondly, alloy design strategy would involve developing light-weight RHEAs with superior mechanical properties at wide-temperature ranges.

II. The second part of the doctorate thesis would include developing targets of developed new alloy compositions and synthesizing RHEFs and its nitride films, and studying its nano-mechanical and high temperature tribological properties. RHEFs and its nitrides tend to have high frictional coefficient. New synthesis strategy would include co-sputtering multi-principal element target with other targets, such as MoS_2 or graphite, to increasing the lubricating properties of RHEFs.

7. References

[1] J.W. Yeh, S.K. Chen, S.J. Lin, J.Y. Gan, T.S. Chin, T.T. Shun, C.H. Tsau, S.Y. Chang, Nanostructured high-entropy alloys with multiple principal elements: Novel alloy design concepts and outcomes, Adv. Eng. Mater. 6 (2004) 299–303+274. doi:10.1002/adem.200300567.

[2] B. Cantor, I.T.H. Chang, P. Knight, A.J.B. Vincent, Microstructural development in equiatomic multicomponent alloys, Mater. Sci. Eng. A. 375–377 (2004) 213–218. doi:10.1016/j.msea.2003.10.257.

[3] S. Ranganathan, Alloyed pleasures : Multimetallic cocktails, Curr. Sci. 85 (2003) 1404–1406.

[4] R.A. Swalin, Thermodynamics of Solids, 2nd Edn., Wiley, NY, 1991.

[5] D.B. Miracle, J.D. Miller, O.N. Senkov, C. Woodward, M.D. Uchic, J. Tiley, Exploration and development of high entropy alloys for structural applications, Entropy. 16 (2014) 494–525. doi:10.3390/e16010494.

[6] D.B. Miracle, O.N. Senkov, A critical review of high entropy alloys and related concepts, Acta Mater. 122 (2017) 448–511. doi:10.1016/j.actamat.2016.08.081.

[7] D.A. Porter, K.. Easterling, S. M.Y, Phase transformation in metals and alloys, 3rd Editio, CRC Press, 2009.

[8] J. Yeh, Recent progress in high-entropy alloys, Ann. Chim. – Sci. Des Mater. 31 (2006) 633–648. doi:10.3166/acsm.31.633-648.

[9] J.W. Yeh, S.K. Chen, S.J. Lin, J.Y. Gan, T.S. Chin, T.T. Shun, C.H. Tsau, S.Y. Chang, Nanostructured high-entropy alloys with multiple principal elements: Novel alloy design concepts and outcomes, Adv. Eng. Mater. 6 (2004) 299–303+274. doi:10.1002/adem.200300567.

[10] B.Y. Zhang, Y.J. Zhou, J.P. Lin, G.L. Chen, P.K. Liaw, Solid-Solution Phase Formation Rules for Multi-component Alloys **, Adv. Eng. Mater. 10 (2008) 534–538. doi:10.1002/adem.200700240.

[11] Z. Yong, Z. Yunjun, H.U.I. Xidong, W. Meiling, C. Guoliang, Minor alloying behavior in bulk metallic glasses and high-entropy alloys, Sci. China Ser. G Physics, Mech. Astron. 51 (2008) 427–437. doi:10.1007/s11433-008-0050-5.

[12] J. Yeh, S. Chen, J. Gan, S. Lin, T. Chin, Formation of Simple Crystal Structures in Cu-Co-Ni-Cr-Al-Fe-Ti-V Alloys with Multiprincipal Metallic Elements, Metall. Mater. Trans. A. 35 (2004) 2533–2536.

[13] J. Yeh, S. Chang, Y. Hong, S. Chen, S. Lin, Anomalous decrease in X-ray diffraction intensities of Cu–Ni–Al–Co–Cr–Fe–Si alloy systems with multi-principal elements, Mater. Chem. Phys. 103 (2007) 41–46. doi:10.1016/j.matchemphys.2007.01.003.

[14] Y.J. Zhou, Y. Zhang, Y.L. Wang, G.L. Chen, Solid solution alloys of AlCoCrFeNiTix with excellent room-temperature mechanical properties, Appl. Phys. Lett. 90 (2007) 181904. doi:10.1063/1.2734517.

[15] J.W. Yeh, Y.L. Chen, S.J. Lin, S.K. Chen, High-Entropy Alloys – A New Era of Exploitation, Mater. Sci. Forum. 560 (2007) 1–9. doi:10.4028/www.scientific.net/MSF.560.1.

[16] P. Huang, J. Yeh, T.-T. Shun, S.-K. Chen, Multi-Principal-Element Alloys with Improved Oxidation and Wear Resistance for Thermal Spray Coating, Adv. Eng. Mater. 6 (2004) 74–78. doi:10.1002/adem.200300507.

[17] C. Hsu, J. Yeh, S. Chen, T. Shun, Wear Resistance and High-Temperature Compression Strength of Fcc CuCoNiCrAl 0 . 5 Fe Alloy with Boron Addition, Metall. Mater. Trans. A. 35A (2004) 1465–1469.

[18] C. Tong, M. Chen, S. Chen, J. Yeh, T. Shun, S. Lin, S. Chang, Mechanical Performance of the Al x CoCrCuFeNi High-Entropy Alloy System with Multiprincipal Elements, 36 (2005) 1263–1271.

[19] O.N. Senkov, G.B. Wilks, D.B. Miracle, C.P. Chuang, P.K. Liaw, Refractory high-entropy alloys, Intermetallics. 18 (2010) 1758–1765. doi:10.1016/j.intermet.2010.05.014.

[20] J.P. Couzinié, G. Dirras, L. Perrière, T. Chauveau, E. Leroy, Y. Champion, I. Guillot, Microstructure of a near-equimolar refractory high-entropy alloy, Mater. Lett. 126 (2014) 285–287. doi:10.1016/j.matlet.2014.04.062.

[21] Y.Y. Chen, T. Duval, U.D. Hung, J.W. Yeh, H.C. Shih, Microstructure and electrochemical properties of high entropy alloys—a comparison with type-304 stainless steel, Corros. Sci. 47 (2005) 2257–2279. doi:https://doi.org/10.1016/j.corsci.2004.11.008.

[22] S. Varalakshmi, M. Kamaraj, B.S. Murty, Synthesis and characterization of nanocrystalline AlFeTiCrZnCu high entropy solid solution by mechanical alloying, J. Alloys Compd. 460 (2008) 253–257. doi:10.1016/j.jallcom.2007.05.104.

[23] B.S. Murty, J.W. Yeh, S. Ranganathan, Chapter 5 - Synthesis and Processing, in: B.S. Murty, J.W. Yeh, S. Ranganathan (Eds.), High Entropy Alloy., Butterworth-Heinemann, Boston, 2014: pp. 77–89.

doi:https://doi.org/10.1016/B978-0-12-800251-3.00005-5.

[24] S. Mohanty, N.P. Gurao, K. Biswas, Sinter ageing of equiatomic Al20Co20Cu20Zn20Ni20 high entropy alloy via mechanical alloying, Mater. Sci. Eng. A. 617 (2014) 211–218. doi:10.1016/j.msea.2014.08.046.

[25] B. Gwalani, R.M. Pohan, J. Lee, B. Lee, R. Banerjee, H.J. Ryu, High-entropy alloy strengthened by in situ formation of entropy- stabilized nano-dispersoids, Sci. Rep. (2018) 1–9. doi:10.1038/s41598-018-32552-6.

[26] B. Kang, J. Lee, H. Jin, S. Hyung, Materials Science & Engineering A Ultra-high strength WNbMoTaV high-entropy alloys with fi ne grain structure fabricated by powder metallurgical process, Mater. Sci. Eng. A. 712 (2018) 616–624. doi:10.1016/j.msea.2017.12.021.

[27] A. Zhang, J. Han, B. Su, J. Meng, A novel CoCrFeNi high entropy alloy matrix self-lubricating composite, J. Alloys Compd. 725 (2017) 700–710. doi:10.1016/j.jallcom.2017.07.197.

[28] S. Cao, J. Zhou, L. Wang, Y. Yu, B. Xin, Microstructure, mechanical and tribological property of multi-components synergistic self-lubricating NiCoCrAl matrix composite, Tribol. Int. (2018). doi:10.1016/j.triboint.2018.10.050.

[29] D. Depla, S. Mahieu, Reactive Sputter Deposition, Springer Berlin Heidelberg, 2008. doi:10.1007/978-3-540-76664-3.

[30] X.H. Yan, J.S. Li, W.R. Zhang, Y. Zhang, A brief review of high-entropy films, Mater. Chem. Phys. 210 (2018) 12–19. doi:10.1016/j.matchemphys.2017.07.078.

[31] W. Li, P. Liu, P.K. Liaw, Microstructures and properties of high-entropy alloy films and coatings: A review, Mater. Res. Lett. 6 (2018) 199–229. doi:10.1080/21663831.2018.1434248.

[32] A.D. Pogrebnjak, V.M. Beresnev, K. V. Smyrnova, Y.O. Kravchenko, P. V. Zukowski, G.G. Bondarenko, The influence of nitrogen pressure on the fabrication of the two-phase superhard nanocomposite (TiZrNbAlYCr)N coatings, Mater. Lett. 211 (2018) 316–318. doi:10.1016/j.matlet.2017.09.121.

[33] S.Y. Lin, S.Y. Chang, Y.C. Huang, F.S. Shieu, J.W. Yeh, Mechanical performance and nanoindenting deformation of (AlCrTaTiZr)NC y multi-component coatings co-sputtered with bias, Surf. Coatings Technol. 206 (2012) 5096–5102. doi:10.1016/j.surfcoat.2012.06.035.

[34] M.I. Lin, M.H. Tsai, W.J. Shen, J.W. Yeh, Evolution of structure and

properties of multi-component (AlCrTaTiZr)Ox films, Thin Solid Films. 518 (2010) 2732–2737. doi:10.1016/j.tsf.2009.10.142.

[35] M. Braic, V. Braic, M. Balaceanu, C.N. Zoita, A. Vladescu, E. Grigore, Characteristics of (TiAlCrNbY)C films deposited by reactive magnetron sputtering, Surf. Coatings Technol. 204 (2010) 2010–2014. doi:10.1016/j.surfcoat.2009.10.049.

[36] Y.S. Jhong, C.W. Huang, S.J. Lin, Effects of CH4flow ratio on the structure and properties of reactively sputtered (CrNbSiTiZr)Cxcoatings, Mater. Chem. Phys. 210 (2018) 348–352. doi:10.1016/j.matchemphys.2017.08.002.

[37] H. Kim, S. Nam, A. Roh, M. Son, M. Ham, J. Kim, H. Choi, Mechanical and electrical properties of NbMoTaW refractory high-entropy alloy thin films, Int. J. Refract. Metals Hard Mater. 80 (2019) 286–291. doi:10.1016/j.ijrmhm.2019.02.005.

[38] S. Fritze, C.M. Koller, L. Von Fieandt, P. Malinovskis, K. Johansson, E. Lewin, P.H. Mayrhofer, U. Jansson, Influence of Deposition Temperature on the Phase Evolution of HfNbTiVZr High-Entropy Thin Films, (2019) 10–17. doi:10.3390/ma12040587.

[39] H.-T. Hsueh, W.-J. Shen, M.-H. Tsai, J.-W. Yeh, Effect of nitrogen content and substrate bias on mechanical and corrosion properties of high-entropy films (AlCrSiTiZr)100−xNx, Surf. Coatings Technol. 206 (2012) 4106–4112. doi:10.1016/j.surfcoat.2012.03.096.

[40] H.W. Chang, P.K. Huang, J.W. Yeh, A. Davison, C.H. Tsau, C.C. Yang, Influence of substrate bias, deposition temperature and post-deposition annealing on the structure and properties of multi-principal-component (AlCrMoSiTi)N coatings, Surf. Coatings Technol. 202 (2008) 3360–3366. doi:10.1016/j.surfcoat.2007.12.014.

[41] P.K. Huang, J.W. Yeh, Effects of substrate temperature and post-annealing on microstructure and properties of (AlCrNbSiTiV)N coatings, Thin Solid Films. 518 (2009) 180–184. doi:10.1016/j.tsf.2009.06.020.

[42] A.D. Pogrebnjak, I. V. Yakushchenko, O. V. Bondar, O. V. Sobol', V.M. Beresnev, K. Oyoshi, H. Amekura, Y. Takeda, Influence of implantation of Au− ions on the microstructure and mechanical properties of the nanostructured multielement (TiZrHf VNbTa)N coating, Phys. Solid State. 57 (2015) 1559–1564. doi:10.1134/S1063783415080259.

[43] Z. Chang, Structure and properties of duodenary (TiVCrZrNbMoHfTaWAlSi) N coatings by reactive magnetron sputtering, Mater. Chem. Phys. 220 (2018) 98–110.

doi:10.1016/j.matchemphys.2018.08.068.

[44] Y. Zou, H. Ma, R. Spolenak, Ultrastrong ductile and stable high-entropy alloys at small scales, Nat. Commun. 6 (2015) 1–8. doi:10.1038/ncomms8748.

[45] Y. Zou, J.M. Wheeler, H. Ma, P. Okle, R. Spolenak, Nanocrystalline High-Entropy Alloys: A New Paradigm in High-Temperature Strength and Stability, Nano Lett. 17 (2017) 1569–1574. doi:10.1021/acs.nanolett.6b04716.

[46] S. Mridha, M. Komarasamy, S. Bhowmick, R.S. Mishra, S. Mukherjee, Small-Scale Plastic Deformation of Nanocrystalline High Entropy Alloy, Entropy. 20 (2018) 1–6. doi:10.3390/e20110889.

[47] L. Gao, W. Liao, H. Zhang, J. Surjadi, D. Sun, Y. Lu, Microstructure, Mechanical and Corrosion Behaviors of CoCrFeNiAl0.3 High Entropy Alloy (HEA) Films, Coatings. 7 (2017) 156. doi:10.3390/coatings7100156.

[48] K.H. Cheng, C.H. Lai, S.J. Lin, J.W. Yeh, Structural and mechanical properties of multi-element (AlCrMoTaTiZr)Nxcoatings by reactive magnetron sputtering, Thin Solid Films. 519 (2011) 3185–3190. doi:10.1016/j.tsf.2010.11.034.

[49] V. Braic, A. Vladescu, M. Balaceanu, C.R. Luculescu, M. Braic, Nanostructured multi-element (TiZrNbHfTa)N and (TiZrNbHfTa)C hard coatings, Surf. Coatings Technol. 211 (2012) 117–121. doi:10.1016/j.surfcoat.2011.09.033.

[50] W.-J. Shen, M.-H. Tsai, J.-W. Yeh, Machining Performance of Sputter-Deposited (Al0.34Cr0.22Nb0.11Si0.11Ti0.22)50N50 High-Entropy Nitride Coatings, Coatings. 5 (2015) 312–325. doi:10.3390/coatings5030312.

[51] V. Bushlya, D. Johansson, F. Lenrick, J. Ståhl, F. Schultheiss, Wear mechanisms of uncoated and coated cemented carbide tools in machining lead-free silicon brass, Wear. 376–377 (2017) 143–151. doi:10.1016/j.wear.2017.01.039.

[52] R. Yu, R. Huang, C. Lee, F. Shieu, Synthesis and characterization of multi-element oxynitride semiconductor film prepared by reactive sputtering deposition, Appl. Surf. Sci. 263 (2012) 58–61.

[53] R. Lin, T. Lee, D. Wu, Y. Lee, A Study of Thin Film Resistors Prepared Using Ni-Cr-Si-Al-Ta High Entropy Alloy, Adv. Mater. Sci. Eng. Article ID (2015) 7 pages.

[54] P.-C. Lin, C.-Y. Cheng, J.-W. Yeh, T.-S. Chin, Soft Magnetic

Properties of High-Entropy Fe-Co-Ni-Cr-Al-Si Thin Films, Entropy. 18 (2016). doi:10.3390/e18080308.

[55] P.K. Huang, J.W. Yeh, Inhibition of grain coarsening up to 1000 C in (AlCrNbSiTiV)N superhard coatings, Scr. Mater. 62 (2010) 105–108. doi:10.1016/j.scriptamat.2009.09.015.

[56] W.J. Shen, M.H. Tsai, K.Y. Tsai, C.C. Juan, C.W. Tsai, J.W. Yeh, Y.S. Chang, Superior Oxidation Resistance of (Al0.34Cr0.22Nb0.11Si0.11Ti0.22)50N50 High-Entropy Nitride, J. Electrochem. Soc. 160 (2013) C531–C535. doi:10.1149/2.028311jes.

[57] Y.F. Ye, Q. Wang, J. Lu, C.T. Liu, Y. Yang, High-entropy alloy: challenges and prospects, Mater. Today. 19 (2016) 349–362. doi:10.1016/j.mattod.2015.11.026.

[58] O.N. Senkov, D.B. Miracle, K.J. Chaput, J.P. Couzinie, Development and exploration of refractory high entropy alloys - A review, J. Mater. Res. 33 (2018) 3092–3128. doi:10.1557/jmr.2018.153.

[59] O.N. Senkov, G.B. Wilks, J.M. Scott, D.B. Miracle, Mechanical properties of Nb25Mo25Ta25W25 and V20Nb20Mo20Ta20W20 refractory high entropy alloy, Intermetallics. 19 (2011) 698–706. doi:10.1016/j.intermet.2011.01.004.

[60] O.N. Senkov, S. V. Senkova, C. Woodward, D.B. Miracle, Low-density, refractory multi-principal element alloys of the Cr-Nb-Ti-V-Zr system: Microstructure and phase analysis, Acta Mater. 61 (2013) 1545–1557. doi:10.1016/j.actamat.2012.11.032.

[61] E.M. Savitskii, G.S. Burkhanov, Physical Metallurgy of Refractory Metals and Alloys, Springer, Boston, MA, 1995. doi:10.1007/978-1-4684-1572-8.

[62] W. Guo, B. Liu, Y. Liu, T. Li, A. Fu, Q. Fang, Y. Nie, Microstructures and mechanical properties of ductile NbTaTiV refractory high entropy alloy prepared by powder metallurgy, J. Alloys Compd. 776 (2019) 428–436. doi:10.1016/j.jallcom.2018.10.230.

[63] T.K. Tsao, A.C. Yeh, C.M. Kuo, K. Kakehi, H. Murakami, J.W. Yeh, S.R. Jian, The High Temperature Tensile and Creep Behaviors of High Entropy Superalloy, Sci. Rep. 7 (2017) 1–9. doi:10.1038/s41598-017-13026-7.

[64] C.C. Juan, M.H. Tsai, C.W. Tsai, C.M. Lin, W.R. Wang, C.C. Yang, S.K. Chen, S.J. Lin, J.W. Yeh, Enhanced mechanical properties of HfMoTaTiZr and HfMoNbTaTiZr refractory high-entropy alloys, Intermetallics. 62 (2015) 76–83. doi:10.1016/j.intermet.2015.03.013.

[65] S. Sheikh, S. Shafeie, Q. Hu, J. Ahlström, C. Persson, J. Veselý, J. Zýka, U. Klement, S. Guo, Alloy design for intrinsically ductile refractory high-entropy alloys, J. Appl. Phys. 120 (2016). doi:10.1063/1.4966659.

[66] N.N. Guo, L. Wang, L.S. Luo, X.Z. Li, R.R. Chen, Y.Q. Su, J.J. Guo, H.Z. Fu, Microstructure and mechanical properties of refractory high entropy (Mo0.5NbHf0.5ZrTi) BCC/M5Si3 in-situ compound, J. Alloys Compd. 660 (2016) 197–203. doi:10.1016/j.jallcom.2015.11.091.

[67] N.N. Guo, L. Wang, L.S. Luo, X.Z. Li, R.R. Chen, Y.Q. Su, J.J. Guo, H.Z. Fu, Microstructure and mechanical properties of in-situ MC-carbide particulates-reinforced refractory high-entropy Mo0.5NbHf0.5ZrTi matrix alloy composite, Intermetallics. 69 (2016) 74–77. doi:10.1016/j.intermet.2015.09.011.

[68] Y. Zhang, Y. Liu, Y. Li, X. Chen, H. Zhang, Microstructure and mechanical properties of a refractory HfNbTiVSi0.5 high-entropy alloy composite, Mater. Lett. 174 (2016) 82–85. doi:10.1016/j.matlet.2016.03.092.

[69] Y. Liu, Y. Zhang, H. Zhang, N. Wang, X. Chen, H. Zhang, Y. Li, Microstructure and mechanical properties of refractory HfMo0.5NbTiV0.5Six high-entropy composites, J. Alloys Compd. 694 (2017) 869–876. doi:10.1016/j.jallcom.2016.10.014.

[70] N.Y. Yurchenko, N.D. Stepanov, S. V Zherebtsov, M.A. Tikhonovsky, G.A. Salishchev, Structure and mechanical properties of B2 ordered refractory AlNbTiVZrx (x=0–1.5) high-entropy alloys, Mater. Sci. Eng. A. 704 (2017) 82–90. doi:10.1016/j.msea.2017.08.019.

[71] N.D. Stepanov, N.Y. Yurchenko, D.G. Shaysultanov, G.A. Salishchev, M.A. Tikhonovsky, Effect of Al on structure and mechanical properties of AlxNbTiVZr (x=0, 0.5, 1, 1.5) entropy alloys, Mater. Sci. Technol. 31 (2015) 1184–1193. doi:10.1179/1743284715Y.0000000032.

[72] O.N. Senkov, S. V Senkova, D.B. Miracle, C. Woodward, Mechanical properties of low-density , refractory multi-principal element alloys of the Cr–Nb–Ti–V–Zr system, Mater. Sci. Eng. A. 565 (2013) 51–62. doi:10.1016/j.msea.2012.12.018.

[73] L. Lilensten, J. Couzinié, J. Bourgon, L. Perrière, G. Dirras, F. Prima, I. Guillot, Design and tensile properties of a bcc Ti-rich high-entropy alloy with transformation-induced plasticity, Mater. Res. Lett. 5 (2017) 110–116. doi:10.1080/21663831.2016.1221861.

[74] H. Huang, Y. Wu, J. He, H. Wang, X. Liu, K. An, W. Wu, Z. Lu,

Phase-Transformation Ductilization of Brittle High-Entropy Alloys via Metastability Engineering, Adv. Mater. 29 (2017) 1–7. doi:10.1002/adma.201701678.

[75] A. Poulia, E. Georgatis, A. Lekatou, A.E. Karantzalis, Microstructure and wear behavior of a refractory high entropy alloy, Int. J. Refract. Met. Hard Mater. 57 (2016) 50–63. doi:10.1016/j.ijrmhm.2016.02.006.

[76] C. Mathiou, A. Poulia, E. Georgatis, A.E. Karantzalis, Microstructural features and dry - Sliding wear response of MoTaNbZrTi high entropy alloy, Mater. Chem. Phys. 210 (2018) 126–135. doi:10.1016/j.matchemphys.2017.08.036.

[77] V. Braic, M. Balaceanu, M. Braic, A. Vladescu, S. Panseri, A. Russo, Characterization of multi-principal-element (TiZrNbHfTa)N and (TiZrNbHfTa)C coatings for biomedical applications, J. Mech. Behav. Biomed. Mater. 10 (2012) 197–205. doi:10.1016/j.jmbbm.2012.02.020.

[78] A.D. Pogrebnjak, I. V. Yakushchenko, A.A. Bagdasaryan, O. V. Bondar, R. Krause-Rehberg, G. Abadias, P. Chartier, K. Oyoshi, Y. Takeda, V.M. Beresnev, O. V. Sobol, Microstructure, physical and chemical properties of nanostructured (Ti-Hf-Zr-V-Nb)N coatings under different deposition conditions, Mater. Chem. Phys. 147 (2014) 1079–1091. doi:10.1016/j.matchemphys.2014.06.062.

[79] X.B. Feng, J.Y. Zhang, Y.Q. Wang, Z.Q. Hou, K. Wu, G. Liu, J. Sun, Size effects on the mechanical properties of nanocrystalline NbMoTaW refractory high entropy alloy thin films, Int. J. Plast. 95 (2017) 264–277. doi:10.1016/j.ijplas.2017.04.013.

[80] X. Feng, J. Zhang, Z. Xia, W. Fu, K. Wu, G. Liu, J. Sun, Stable nanocrystalline NbMoTaW high entropy alloy thin films with excellent mechanical and electrical properties, Mater. Lett. 210 (2018) 84–87. doi:10.1016/j.matlet.2017.08.129.

[81] N. Tüten, D. Canadinc, A. Motallebzadeh, B. Bal, Intermetallics Microstructure and tribological properties of TiTaHfNbZr high entropy alloy coatings deposited on Ti e 6Al e 4V substrates, Intermetallics. 105 (2019) 99–106. doi:10.1016/j.intermet.2018.11.015.

[82] Y. Zou, Nanomechanical studies of high-entropy alloys, J. Mater. Res. 33 (2018) 3035–3054. doi:10.1557/jmr.2018.155.

Department of Engineering Sciences and Mathematics
Division of Materials Science

ISSN 1402-1757
ISBN 978-91-7790-394-9 (print)
ISBN 978-91-7790-395-6 (pdf)

Luleå University of Technology 2019

LULEÅ
UNIVERSITY
OF TECHNOLOGY